Fail-safe design for large capacity lithium-ion battery systems

Gi-Heon Kim*, Kandler Smith, John Ireland, Ahmad Pesaran

National Renewable Energy Laboratory, 1617 Cole Blvd., Golden, CO, USA

ABSTRACT

A fault leading to a thermal runaway in a lithium-ion battery is believed to grow over time from a latent defect. Significant efforts have been made to detect lithium-ion battery safety faults to proactively facilitate actions minimizing subsequent losses. Scaling up a battery greatly changes the thermal and electrical signals of a system developing a defect and its consequent behaviors during fault evolution. In a large-capacity system such as a battery for an electric vehicle, detecting a fault signal and confining the fault locally in the system are extremely challenging. This paper introduces a fail-safe design methodology for large-capacity lithium-ion battery systems. Analysis using an internal short circuit response model for multi-cell packs is presented that demonstrates the viability of the proposed concept for various design parameters and operating conditions. Locating a faulty cell in a multiple-cell module and determining the status of the fault's evolution can be achieved using signals easily measured from the electric terminals of the module. A methodology is introduced for electrical isolation of a faulty cell from the healthy cells in a system to prevent further electrical energy feed into the fault. Experimental demonstration is presented supporting the model results.

© 2012 Elsevier B.V. All rights reserved.

1. Introduction

Lithium-ion batteries (LIBs) are promising candidates for electric energy storage for electric drive vehicles due to their high power and energy density. However, violent incidents reported for this technology [1] and consequent safety concerns are still the major hindrance for fast market penetration of LIB-powered electric drive vehicles. High temperatures can trigger exothermic chemical decomposition of LIB component materials [2,3] that lead to further temperature rise and possible catastrophic failure of the LIB system, which is known as thermal runaway. The unsafe high trigger temperatures may be reached due to a variety of failure scenarios; including overcharge of an individual cell or the entire LIB system; an internal short circuit (ISC) of cells resulting from a latent defect due to an internal foreign object, separator wearout, dendrite growth, or crushing or penetration of a cell; an external short of cells, module or pack; and/or exposure to abnormal high temperature due to fire or failure of neighboring components [4–8].

Mature small-capacity LIBs used in consumer electronics applications ensure safety with multiple redundant layers of incident prevention methods such as positive temperature coefficient devices, current interrupt devices, and shutdown separators. Unfortunately, these safety technologies developed for small-capacity LIB systems do not function properly with large-capacity

LIBs [1]. The LIBs powering electric drive vehicles are significantly larger in capacity and physical size than LIBs for personal electronics, and scaling up LIBs dramatically changes their behaviors under safety incidents. Large-capacity LIB systems are typically made by configuring multiple individual cells into a module or a pack electrically and thermally. It has been generally attempted to address the anticipated safety issues comprehensively at the cell level, and LIB safety characteristics are often well understood at the individual cell level through intense analysis and testing. However, larger batteries, high-capacity and high-voltage assemblies of individual cells, change their response to a fault greatly, causing unexpected subsequent behaviors. Because pack responses are critically affected by pack integration architecture in a complex relation with the characteristics of unit cells, pack-level safety assessments are extremely difficult and expensive in terms of cost and time. The issues and difficulties in the development of safe large LIB systems are identified as:

1.1. Early detection

A fault leading to a field accident of a LIB is believed to grow from a latent defect over time. Therefore, significant efforts have been invested to develop methodologies to detect safety faults of LIBs in their early stages [9–11]. Early detection of the safety faults is believed to allow proactive actions that can minimize subsequent losses. However, detecting the fault signals in large LIB systems is much more difficult than in small LIB systems. As discussed in [6], the thermal response of a LIB cell developing an ISC varies
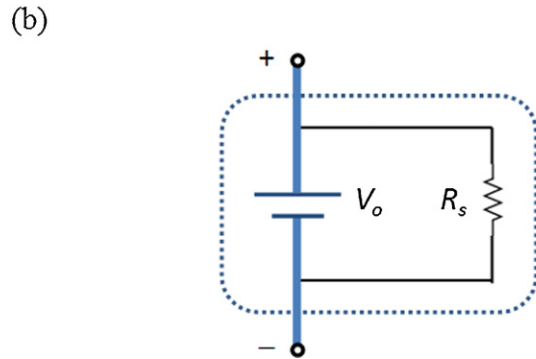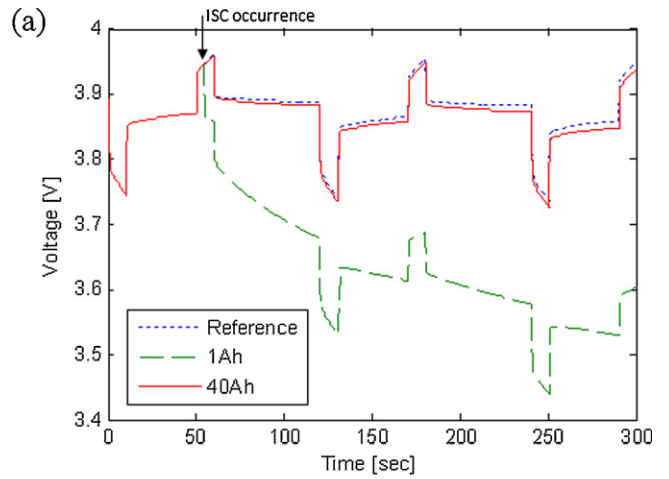
* Corresponding author. Tel.: +1 303 275 4437; fax: +1 303 275 4415.
E-mail address: gi-heon.kim@nrel.gov (G.-H. Kim).

(a)

(b)
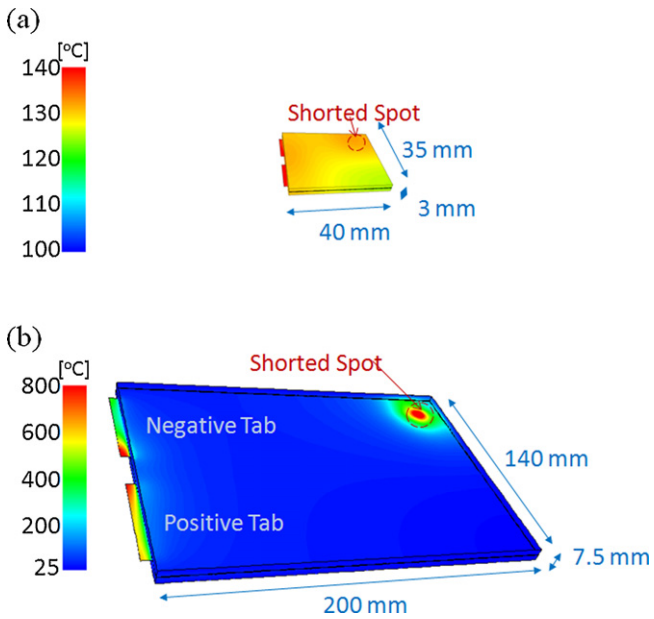
Fig. 1. Illustration of typical pattern of early thermal response of LIB cell developing a low-impedance ISC; (a) simulated temperature field in a 0.4-Ah stacked prismatic cell, (b) Simulated temperature field in a 20-Ah stacked prismatic cell (Ref. [6]).

(a)

(b)

Fig. 2. (a) Model result comparison for output voltage responses of large (40-Ah) and small (1-Ah) capacity cells during pulse cycling (10 s 5 C discharge–40 s rest–10 s 3 C charge–60-s rest); 1-Ω ISC occurs during the first charge pulse at $t = 55$ s; initial SOC is set as 0.8 and (b) schematics of short-circuit cell model used in this study.

substantially depending on its capacity. In small-capacity cells, the entire cell volume is likely heated up by a low resistance ISC due to the high rate of electrical discharge heat, as illustrated in Fig. 1a. A temperature sensor can detect a temperature change and send a fault signal to the LIB controller. In large-capacity cells, however, a highly localized temperature excursion is likely to occur at the region close to the ISC due to the large electrical current convergence. For a large cell, most of the cell volume remains within the normal temperature range, as shown in Fig. 1b. Because of the localized heating pattern of a short, probing a temperature change as a fault signal in large-capacity cells requires exceptionally high-resolution spatial sensing that is impractical to apply in production LIB systems.

Since individual cell voltages are typically well monitored in LIBs for cell balancing purposes, utilizing the voltage signals for detection of safety faults occurring in a system has also been investigated and could work for small-capacity systems [12]. Scaling up battery capacity, however, reduces the viability of using these voltage signals for early-stage fault detection. In Fig. 2a, model simulation results of LIB cell output voltage responses are compared for 1-Ah and 40-Ah cells for the case where an ISC occurs during pulse cycling of each cell. Schematics in Fig. 2b show the short-circuit cell model used in this study. The electric response of a LIB cell is predicted by resolving lithium diffusion dynamics and charge

transfer kinetics [13] using a model reduction technique [14]. The equations that govern the model and the input parameters are summarized in Tables 1 and 2, respectively. When a 1-Ω resistance ISC occurs during the first charge pulse, the output voltage of a 1-Ah cell deviates significantly from its reference voltage due to the internal discharge. Therefore, using this voltage offset as an ISC fault signal is attainable in this case. However, with the 40-Ah cell, the magnitude of the voltage offset from its reference value is greatly reduced because of that cell's smaller impedance. In addition, the large electric charge capacity of the 40-Ah cell slows down the change of the state of charge (SOC) for internal discharge, resulting in a slow change of voltage. Therefore, it takes a longer time for the voltage offset in a large-capacity cell to grow to a meaningful magnitude for detection while the heat for an evolving ISC is

Table 1
Model-governing equations.

Conservation equations:	Boundary conditions:	
Charge, electrolyte phase	$\frac{\partial}{\partial x}\left(\kappa^{\text{eff}}\frac{\partial}{\partial x}\phi_e\right) + \frac{\partial}{\partial x}\left(\kappa_D^{\text{eff}}\frac{\partial}{\partial x}\ln c_e\right) + j^{\text{Li}} = 0 \quad (1)$	$\frac{\partial\phi_e}{\partial x}\Big|_{x=0} = \frac{\partial\phi_e}{\partial x}\Big|_{x=L} = 0$
Charge, solid phase	$\frac{\partial}{\partial x}\left(\sigma^{\text{eff}}\frac{\partial}{\partial x}\phi_s\right) - j^{\text{Li}} = 0 \quad (2)$	$-\sigma_-^{\text{eff}}\frac{\partial\phi_s}{\partial x}\Big|_{x=0} = \sigma_+^{\text{eff}}\frac{\partial\phi_s}{\partial x}\Big|_{x=L_-+L_{\text{sep}}+L_+} = \frac{I}{A}, \quad \frac{\partial\phi_s}{\partial x}\Big|_{x=L_-} = \frac{\partial\phi_s}{\partial x}\Big|_{x=L_-+L_{\text{sep}}} = 0$
Species, electrolyte phase	$\frac{\partial(\varepsilon_e c_e)}{\partial t} = \frac{\partial}{\partial x}\left(D_e^{\text{eff}}\frac{\partial}{\partial x}c_e\right) + \frac{1-t_+^0}{F}j^{\text{Li}} \quad (3)$	$\frac{\partial c_e}{\partial x}\Big|_{x=0} = \frac{\partial c_e}{\partial x}\Big|_{x=L} = 0$
Species, solid phase	$\frac{\partial c_s}{\partial t} = \frac{D_s}{r^2}\frac{\partial}{\partial r}\left(r^2\frac{\partial c_s}{\partial r}\right) \quad (4)$	$\frac{\partial c_s}{\partial r}\Big|_{r=0} = 0, D_s\frac{\partial c_s}{\partial r}\Big|_{r=R_s} = \frac{-j^{\text{Li}}}{a_s F}$
Constitutive relations:		
Diffusional conductivity	$\kappa_D^{\text{eff}} = \frac{2RT\kappa^{\text{eff}}}{F}(t_+^0 - 1)\left(1 + \frac{d\ln f_\pm}{d\ln c_e}\right) \quad (5)$	
	$j^{\text{Li}} = a_s i_0\left\{\exp\left[\frac{\alpha_a F}{RT}\eta\right] - \exp\left[-\frac{\alpha_c F}{RT}\eta\right]\right\} \quad (6)$	
Kinetics	$\eta = \phi_s - \phi_e - U \quad (7)$	
	$i_0 = k(c_e)^{\alpha_a}(c_{s,\text{max}} - c_{s,e})^{\alpha_a}(c_{s,e})^{\alpha_c} \quad (8)$	
Bruggeman relations	$\kappa^{\text{eff}} = \kappa\varepsilon_e^p, D_e^{\text{eff}} = \kappa D_e^p, \sigma^{\text{eff}} = \sigma\varepsilon_s \quad (9\text{--}10)$	

Table 2
Model parameters.

Parameter	Li_xC_6 electrode	Separator	$Li_y(NCA)O_2$ electrode
Thickness, δ [m]	70.0×10^{-6}	25×10^{-6}	50.0×10^{-6}
Volume fraction active, ε_s	0.51		0.41
Volume fraction electrolyte, ε_e	0.4	0.4	0.4
Maximum Li capacity, $c_{s,max}$ [mol m^{-3}]	2.87×10^4		4.90×10^4
Specific area, a_s [m^2 m^{-3}]	3.010×10^6		0.753×10^6
Characteristic diffusion length, R_s [m]	5.083×10^{-6}		1.6334×10^{-6}
Stoichiometry at 0% SOC, $x_{0\%}, y_{0\%}$	0.0712		0.98
Stoichiometry at 100% SOC, $x_{100\%}, y_{100\%}$	0.63		0.41
Exchange current density, i_0 [A m^{-2}]	36.0		4.0
- Activation energy, $E_{act}^{i_0}$ [J mol^{-1}]	3.0×10^4		3.0×10^4
Charge-transfer coefficients, α_a, α_c	0.5, 0.5		0.5, 0.5
Film resistance, R_{film} [Ω m^2]	0		0
Solid diffusion coefficient, D_s [m^2 s^{-1}]	9.0×10^{-14}		3×10^{-15}
- Activation energy, $E_{act}^{D_s}$ [J mol^{-1}]	4.0×10^3		2.0×10^4
Solid conductivity, σ [S m^{-1}]	100.0		10
Bruggeman tortuosity exponent, p	2.0	2.0	2.0
Electrolyte concentration, c_e [mol m^{-3}]	1.2×10^3		
Electrolyte phase Li$^+$ diffusion coefficient, D_e [m^2 s^{-1}]	$D_e = 5.84 \times 10^{-7} \ \exp[-2870/T](c_e/1000)^2$ $-33.9 \times 10^{-7} \ \exp[-2920/T](c_e/1000)$ $+129 \times 10^{-7} \ \exp[-3200/T]$		
Electrolyte ionic conductivity, κ [S m^{-1}]	$\kappa = 3.45 \exp[-798/T](c/1000)^3$ $-48.5 \exp[-1080/T](c/1000)^2$ $+244 \exp[-1440/T](c/1000)$		
Li$^+$ transference number, t_+^0	$t_+^0 = -0.000267 \exp[883/T](c_e/1000)^2$ $+0.00309 \ \exp[653/T](c_e/1000)$ $+0.517 \ \exp[-49.6/T]$		
Thermodynamic factor, $\partial \ln f_{\pm}/\partial \ln c_e$	0		

Parameter	Value
Negative electrode, U_- [V]	$U_-(x) = 0.124 + 1.5 \exp(-70x) - 0.0351 \tanh\left(\dfrac{x - 0.286}{0.083}\right) - 0.0045 \ \tanh\left(\dfrac{x - 0.9}{0.119}\right)$ $-0.035 \ \tanh\left(\dfrac{x - 0.99}{0.05}\right) - 0.0147 \ \tanh\left(\dfrac{x - 0.5}{0.034}\right) - 0.102 \ \tanh\left(\dfrac{x - 0.194}{0.142}\right)$ $-0.022 \tanh\left(\dfrac{x - 0.98}{0.0164}\right) - 0.011 \ \tanh\left(\dfrac{x - 0.124}{0.0226}\right) + 0.0155 \ \tanh\left(\dfrac{x - 0.105}{0.029}\right)$
Positive electrode, U_+ [V]	$U_+ = 1.638 x^{10} - 2.222 x^9 + 15.056 x^8 - 23.488 x^7 + 81.246 x^6$ $-344.566 x^5 + 621.3475 x^4 - 554.774 x^3 + 264.427 x^2 - 66.3691 x$ $+11.8058 - 0.61386 \exp(5.8201 x^{136.4})$

accumulating in a cell. A typical battery management system incorporates fast-computing, low-fidelity circuit analogy models as an on-board battery reference model. Together with the small magnitude of the signal, the uncertainty of the reference value is another factor making it difficult to use voltage offset for timely detection of a fault in large-capacity LIB systems.

### 1.2. Electrical isolation

Using circuit-breakers, electrical isolation of a fault is well practiced in various electrical systems to prevent further electrical current feed energizing the fault. However, neither an active circuit-breaker nor a passive circuit-breaker is easily applicable to a large-capacity LIB system. Enacting an active circuit-breaker such as a switch should be preceded by sensing an occurrence of a fault. The difficulty of timely fault detection hinders adopting active circuit-breakers in large LIBs. Passive circuit-breakers such as fuses or positive temperature coefficient devices limit the fault current by opening the circuit when abnormally excessive current flows through the device. In large-capacity LIB systems, a fault electric current, even though it can be a large current, will not be excessively larger than the system's normal operating current. Large-capacity LIBs carry a large operating current when delivering or storing high

electric power. Therefore, properly applying or designing passive circuit breakers triggered by abnormally excessive current is not easy with large LIB systems.

In this paper, a fail-safe design for large-capacity LIB systems is suggested that addresses the issues and the difficulties discussed in this section. A pack ISC response model is developed to investigate the viability of the proposed concept against various design parameters and operation conditions.

2. A fail-safe design for large LIBs

In conventional LIBs, electrode active material particles are mixed with a conductive agent, and the composite slurry is coated onto highly conductive metal current collector sheets that are welded to connections with the cell negative and positive terminals. In a system consisting of multiple cells, electric interconnectors join the cell terminals, forming electric configurations among individual cell units. When a charge transfer reaction occurs at the reaction sites of the active particle surfaces, the electric current is carried through the electrical conduction pathways constructed between active particles and a system terminal. The roles of the electrical pathways in a LIB system are to:
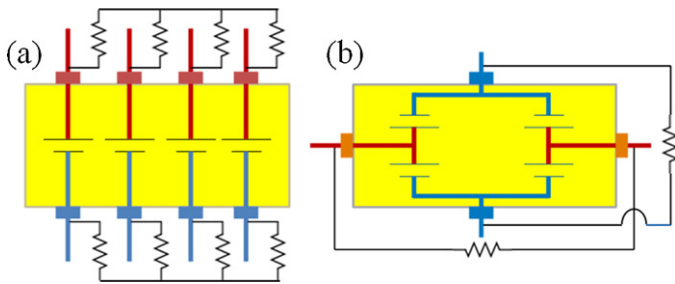
Fig. 3. Conceptual diagram of proposed design facilitating methodologies for enhancement of large-capacity LIB safety: (a) laterally connected configuration and (b) cross-connected configuration.

1) deliver battery electric power during charge and discharge of a LIB system, and
2) keep balance within a LIB system to maximize material utilization and to prolong life.

Our proposed design separates these two distinct functions of electrical pathways in LIBs to facilitate methodologies for enhancing large-capacity LIB safety. Large-capacity LIBs carry a large current while releasing or storing electric energy. Therefore, to avoid excessive loss causing inefficiency in a system, electric current pathways should be designed to be as conductive as possible. In conventional LIB systems, the same conductive pathways are also used for carrying balancing current to achieve fast balancing across the systems. However, pathways for balancing current do not necessarily need to be as conductive as the pathways that carry battery power current, since the balancing current is much smaller in magnitude than the typical charge or discharge current of large LIBs. The proposed fail-safe design for large LIB systems incorporates relatively resistive balancing lines while having conductive power lines. Fig. 3 presents two possible representations of the concept. This concept can be realized in various forms by externally integrating individual unit cells or by having multiple, electrically discrete jelly-rolls in a single cell container. This design has distinct safety advantages that address the issues listed in the previous section.

2.1. Increasing the fault signal in large LIBs

Fig. 4 illustrates one embodiment of the fail-safe concept, configured with two lateral (Fig. 3a) series branches and resistive balancing lines connecting parallel cell elements. The design with two lateral series branches is chosen here for ease of explanation, though the general concept extends to an arbitrary number of branches connected in parallel using resistive balancing lines. Illustrations of module discharge current flow are shown for a well-balanced module in Fig. 4a and for a module developing an ISC in Fig. 4b. In a balanced, healthy battery module, the two conductive series branches are expected to carry identical amounts of electric current so that the current measured from each series branch should be same at both the positive and the negative terminals of the module. On the other hand, when an ISC is induced in one of the cells integrated in the module, the terminal currents measured from the series branches will depart from the balance. Because the resistive parallel connections of the module may not be able to offset the abrupt imbalance immediately carrying a relatively small current, a significant portion of the balancing current will flow along the conductive series connection loop increasing the fault signal at the module terminals.

Here we propose using a departure of the terminal current from its balance as a fault signal applicable in large-capacity batteries. For an arbitrary number of parallel branches, the fault signal is the difference between each branch current and the average current of
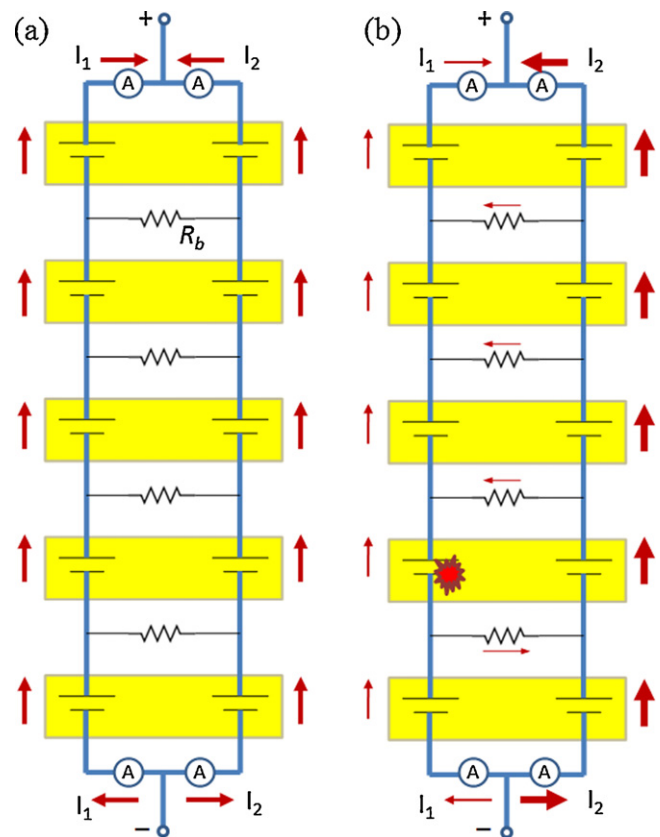
Fig. 4. Schematics of a multi-cell LIB module configured with two lateral series branches and resistive balancing lines across parallel unit cells. Representations of module discharge current flow (a) in a well-balanced module, and (b) in a module developing an ISC.

all branches (the same as the total current divided by the number of branches). For the case of the two branches shown in Fig. 4, the fault signal (FS) is the difference between the two branch currents,

$$FS = I_2 - I_1 \tag{1}$$

Using this quantity for detection of a fault in a battery module composed of multiple cells has several advantages:

1) The magnitude of the signal is typically large enough even for early-stage high-impedance ISC detection.
2) The reference value of the signal is readily known.
3) The signal measured at the module terminals can determine the fault occurrence in any component cell of the module.

The uncertainty of conventional reference models for LIB systems causes difficulty in using output voltage as a fault signal. The issue with the uncertainty of a reference model can be accounted for in the design proposed here. In a well-balanced module, the reference value of the fault signal suggested is known regardless of whether the system is at rest or undergoing charge/discharge cycling ($FS_{ref} = 0$ for Eq. (1)). While current measurement sensors can add expense to the system, only a few measurements at the module terminals can monitor the fault behavior of the entire module. Therefore, a large amount of cell-by-cell high spatial resolution sensing is not required by the proposed concept.

3. Pack ISC simulation

Computer simulations of the electrical response of a pack developing an ISC are performed to evaluate the viability of the proposed
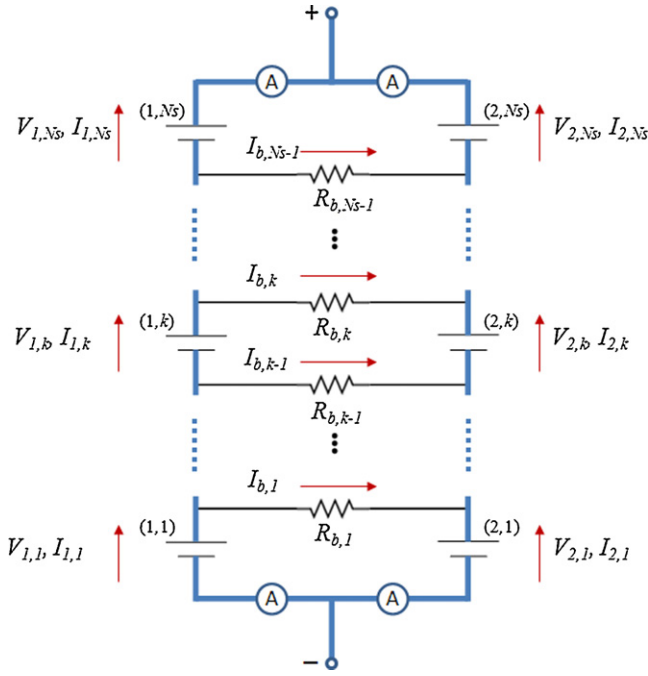
Fig. 5. Circuit diagram of a two-branch module with N_s cells in series and the number notation of calculated quantities.

concept and to investigate the impacts of the system design parameters and operating conditions.

3.1. Pack ISC response model

A pack ISC response model is developed for the two-branch module shown in Fig. 5, where the number of cells in series is N_s, to investigate the viability of the proposed concept against various design parameters and operating conditions. Current conservation at the nodes of the module gives:

$$I_{1,1} + I_{2,1} = I_{mdl} \tag{2}$$

$$I_{1,k+1} + I_{b,k} = I_{1,k} \quad (k = 1, 2, \ldots, N_s - 1) \tag{3}$$

$$I_{2,k+1} = I_{b,k} + I_{2,k} \quad (k = 1, 2, \ldots, N_s - 1) \tag{4}$$

where I_{mdl} is the output current at the module terminals. Energy conservation yields Kirchhoff's loop rule:

$$V_{1,1} - I_{b,1}R_{b,1} = V_{2,1} \tag{5}$$

$$V_{1,k} - I_{b,k}R_{b,k} = V_{2,k} - I_{b,k-1}R_{b,k-1} \quad (k = 2, \ldots, N_s - 1) \tag{6}$$

$$V_{1,Ns} = V_{2,Ns} - I_{b,Ns-1}R_{b,Ns-1} \tag{7}$$

where $R_{b,k}$ is the resistance of the parallel balancing lines. Voltage–current relations are evaluated using the cell model suggested in Fig. 2b and Tables 1 and 2.

3.2. Impact of ISC resistance on fault signal

It is desirable to detect an ISC in the early stages when its electrical resistance is still relatively high and before it evolves into a low-resistance hard short. Therefore, it is important to know how the signal from the proposed design of a LIB system changes while the ISC varies in a system. Fig. 6 presents the impact of ISC resistance on the fault signal suggested in Eq. 1 in the two-branch module in Fig. 5. The signals at the positive and negative module terminals are plotted over time for a 0.1-Ω ISC in Fig. 6a, for a 0.5-Ω ISC in Fig. 6b, and for a 2-Ω ISC in Fig. 6c. The capacity of the simulated module is 40 Ah (20 Ah + 20 Ah). The number of cells in series connection in the module is five. ISCs occur at 5 s in cell (1,2), which is the second cell in the series from the negative terminal in the first branch as notated in Fig. 5. 0.1-Ω resistors are placed in the parallel balancing lines. The module is at rest without charging or discharging during the simulated event. As shown in Fig. 5, the magnitude of the signal is a strong function of the resistance of the induced ISC. Therefore, a pre-developed database providing the relationship between the signal and the resistance of an ISC can be used to determine the status of ISC evolution from an on-board control system. The sign of the signal tells in which branch the ISC has occurred.

3.3. Impact of module output current on fault signal

A viable signal of a fault should be detectable regardless of the use of a battery system. Simulated fault signals for a 0.1-Ω ISC are compared for a module at rest in Fig. 7a, for a module at 3C-discharging in Fig. 7b, and for a module at 3C-charging in Fig. 7c. Other conditions are kept the same as in the previous case. The model results show that the module output current does not greatly affect the signal. Therefore, the signal database for system control is not necessarily developed as a function of a module's output current. For example, a data set collected from a module staying at rest can be applied to detection of a fault occurring in a module being cycled or a module being charged.

3.4. Impact of number of cells in series in a module on fault signal

Simulation results of fault signals at the positive and negative terminals are shown for a module with 5-series cell strings in Fig. 8a, for a module with 10-series cell strings in Fig. 8b, and for a module with 20-series cell strings in Fig. 8c. Other conditions are kept the same as in the previous case. The magnitude of the signal decreases slowly as the number of cells in series in a module increases. This
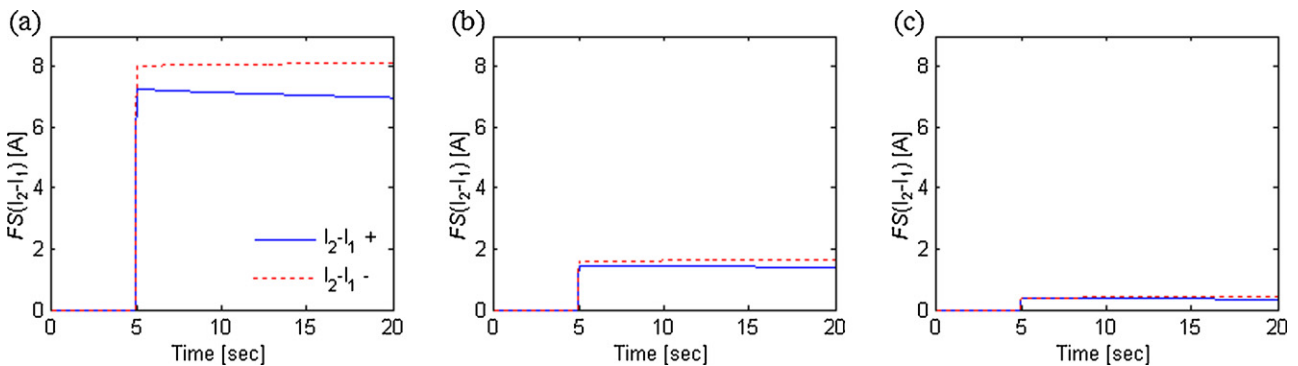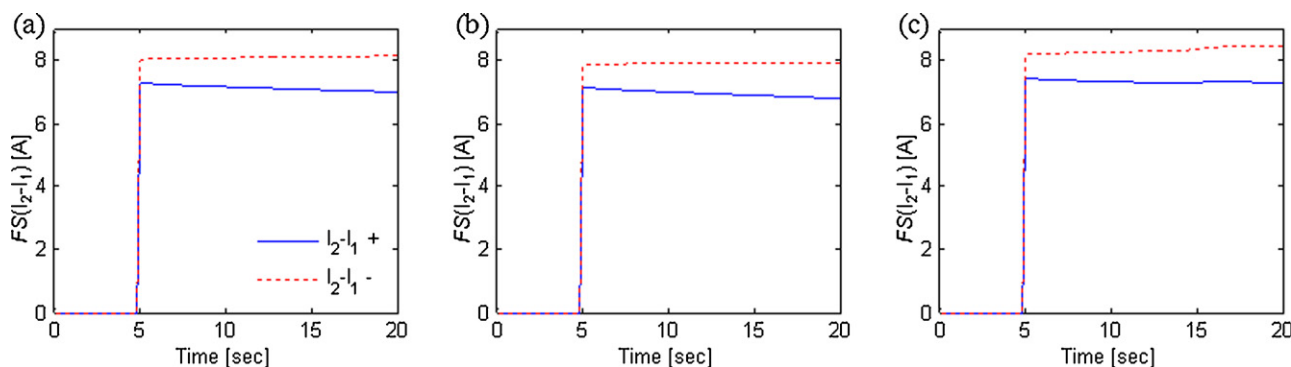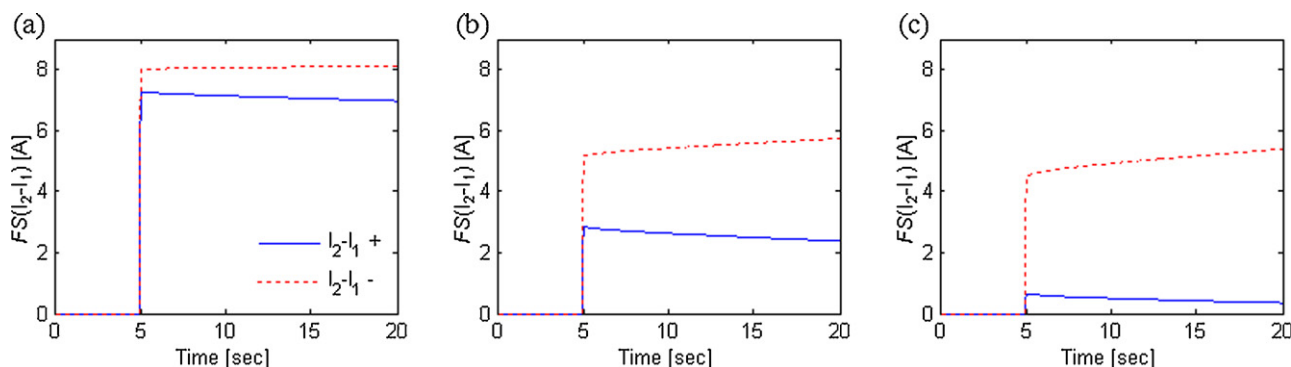

Fig. 6. Pack ISC simulation results of fault signals (FS) at positive and negative module terminals (a) for a 0.1-Ω ISC, (b) for a 0.5-Ω ISC, and (c) for a 2-Ω ISC. For all cases, the ISC occurs at 5 s in cell (1,2) of each module with conditions C_{mdl} = 40 Ah (20 Ah + 20 Ah), I_{mdl} = 0 A, N_s = 5, R_b = 0.1 Ω.

Fig. 7. Pack ISC simulation results of fault signals (FS) at positive and negative module terminals (a) for $I_{mdl} = 0$ A, (b) for $I_{mdl} = 120$ A, and (c) for $I_{mdl} = -120$ A. For all cases, the ISC occurs at 5 s in cell (1,2) of each module with conditions $C_{mdl} = 40$ Ah (20 Ah + 20 Ah), $N_s = 5$, $R_b = 0.1$ Ω, $R_s = 0.1$ Ω.

Fig. 8. Pack ISC simulation results of fault signals (FS) at positive and negative module terminals (a) for $N_s = 5$, (b) for $N_s = 10$, and (c) for $N_s = 20$. For all cases, the ISC occurs at 5 s in cell (1,2) of each module with conditions $C_{mdl} = 40$ Ah (20 Ah + 20 Ah), $I_{mdl} = 0$ A, $R_b = 0.1$ Ω, $R_s = 0.1$ Ω.

is mainly due to the module impedance increase as more cells are added in the series string. The simulation results shown in Fig. 8 indicate that the signals from a module with 20 cells in series are still comparably large enough for the signal from a module with five cells in series.

3.5. Impact of location of a faulted cell in a module on fault signal
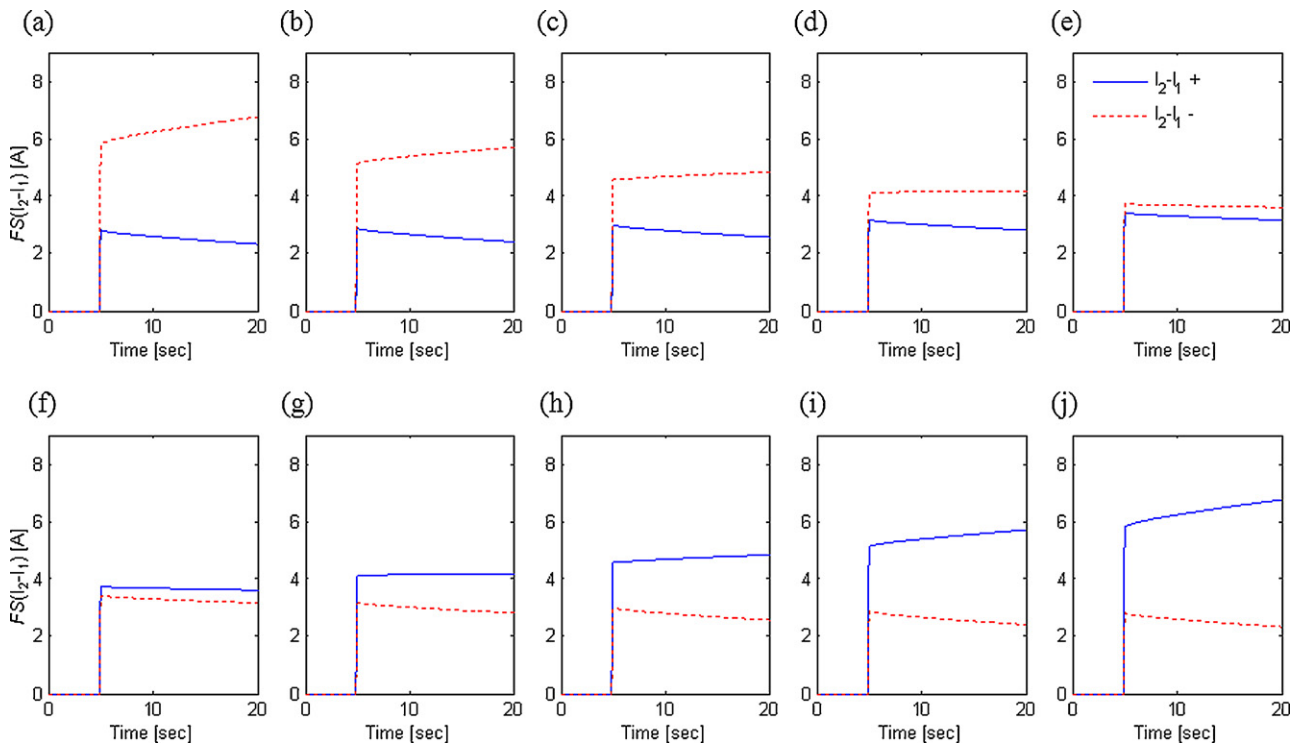
Simulation results of fault signals at positive and negative terminals are presented in Fig. 9 for comparison to show the impact of faulty cell location in a module. The simulations are performed for a 40 Ah module with ten cells in series. The signal is larger at the terminal closer to the faulted cell, because less number of balance paths is available around a faulted cell. For example, when a fault occurs at the cell directly connected to the negative terminal (the case shown in Fig. 9a), the negative terminal signal is measured much larger than the positive terminal signal. Likewise, the signal at the positive terminal is largest for a fault occurring at cell (1,10) seen in Fig. 9j among the cases shown. On the other hand, if a faulty cell is located in the middle of the module (e.g. the case shown in Fig. 9e or f), the magnitudes of the fault signals at the positive and the negative terminals are close to each other. The ratio of the suggested fault signals at the positive terminal and the negative terminal varies with the location of a faulted cell in a module. In general, only two signals are measured at the terminals of a module consisting of two parallel branches with arbitrary number of unit cells. However, the combination of the signals provides the information for identifying the faulted cell in modules including many numbers of cells. Locating and isolating the defective cell in a module will allow a better chance to address the fault locally.

3.6. Impact of capacity and rate capability of a module on fault signal

Requirements for energy content and the maximum power of a LIB system vary with the characteristics of the applications and operational strategy. The power-to-energy ratio of LIBs is typically established by selection of an appropriate unit cell design. In Fig. 10, the impact of the module capacity and rate capability on the fault signal is examined. Fig. 10a–c shows simulated fault signals for modules using the nominal cell designs specified in Tables 1 and 2. The module capacities are 40 Ah (20 Ah + 20 Ah) in Fig. 10a, 10 Ah (5 Ah + 5 Ah) in Fig. 10b, and 4 Ah (2 Ah + 2 Ah) in Fig. 10c. The pulse resistance of these nominal module designs is 2 mΩ m^2 from the pulse discharge simulation. In Fig. 10d–f, model parameters are modified to simulate a low-power module design with a pulse resistance of 8 mΩ m^2. As discussed earlier, detection of a fault in a LIB by sensing a temperature excursion (Fig. 1) or output voltage change (Fig. 2) is extremely challenging for large-capacity and high-power systems. The fault signal proposed in this study, however, is easily detected for the larger-capacity and higher-power modules. Fig. 10 shows that the average magnitude of the signal increases with the capacity and the power rate of the battery.

3.7. Impact on joule heating for short current through ISC

The resistive parallel connections across the conductive series branches in the proposed design effectively limit the amount of current offsetting the imbalance caused by an ISC. This greatly slows down the rate at which electrical energy is fed into a faulty cell from the other, healthy cells in a module. In the event of an ISC, various

Fig. 9. Pack ISC simulation results of fault signals (*FS*) at positive and negative module terminals for ISC occurs at 5 s (a) in cell (1,1); (b) in cell (1,2); (c) in cell (1,3); (d) in cell (1,4); (e) in cell (1,5); (f) in cell (1,6); (g) in cell (1,7); (h) in cell (1,8); (i) in cell (1,9); and (j) in cell (1,10) of a module where $N_s = 10$, $C_{mdl} = 40$ Ah (20 Ah + 20 Ah), $I_{mdl} = 0$ A, $R_b = 0.1$ Ω, $R_s = 0.1$ Ω.
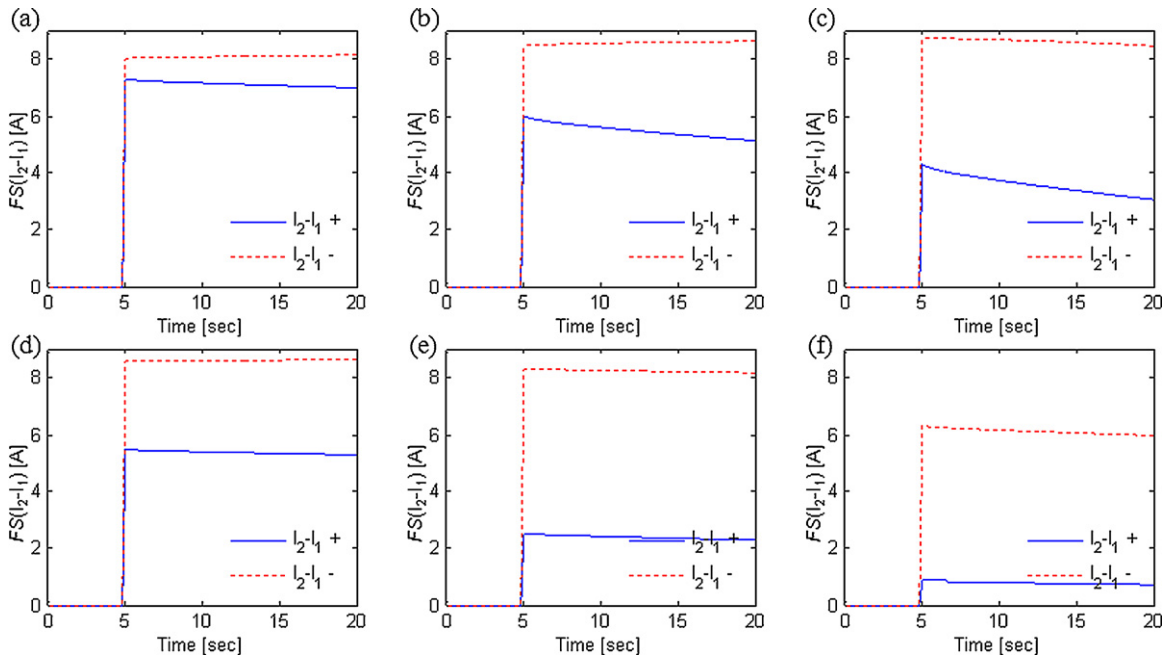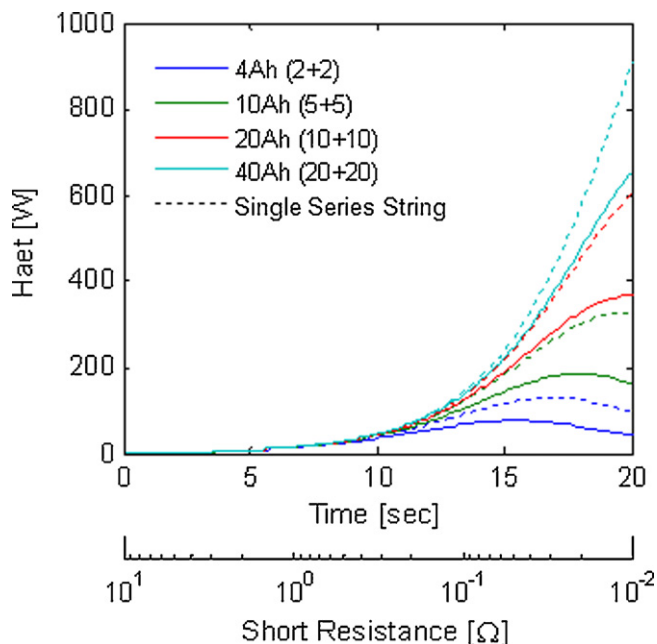

Fig. 10. Pack ISC simulation results of fault signals (*FS*) in a power cell module with 2-mΩ m² pulse resistance (a) for $C_{mdl} = 40$ Ah (20 Ah + 20 Ah), (b) for $C_{mdl} = 10$ Ah (5 Ah + 5 Ah), and (c) for $C_{mdl} = 4$ Ah (2 Ah + 2 Ah); in an energy cell module with 8 mΩ m² pulse resistance (d) for $C_{mdl} = 40$ Ah (20 Ah + 20 Ah), (e) for $C_{mdl} = 10$ Ah (5 Ah + 5 Ah), and (f) for $C_{mdl} = 4$ Ah (2 Ah + 2 Ah). For all cases, the ISC occurs at 5 s in cell (1,2) of each module with conditions $N_s = 5$, $I_{mdl} = 0$ A, $R_b = 0.1$ Ω, $R_s = 0.1$ Ω.

sources of heat such as joule heat due to electrical current converging at the short, electrochemical heat due to cell discharge, and heat released from exothermic decompositions, contribute to temperature increase in the system. Joule heat in conductive elements carrying the short current is typically localized close to a fault and is responsible for the initial thermal behavior of a system. Fig. 11 presents the pack ISC simulation results of short-circuit joule heat

for evolving ISCs in modules developing an ISC. The electrical resistance of a short will likely change with time, dictated by relations among component material properties and cell design characteristics. In the simulations shown in Fig. 11, a temporal function is arbitrarily chosen to represent ISC evolution with time,

$$R_s = 10^{(1-(3t/20))} \ \Omega. \tag{8}$$

Fig. 11. Pack ISC simulation results of short-circuit joule heat for an evolving ISC in modules with various capacities (indicated by colors) where ISC is induced in cell (1,2); $N_s = 5$, $I_{mdl} = 0$ A, $R_b = 0.1$ Ω (solid lines) and $R_b = 0$ Ω (dotted lines).

Fig. 12. Schemes for electrical isolation of a fault in the proposed concept.

In Eq. (8), the short resistance decreases exponentially from 10 Ω to 0.01 Ω during 20 s of simulation time. Fig. 11 compares ISC joule heat for two-branch modules with various capacities. Each case is also compared with ISC joule heat from single-string modules of the same capacities. The simulation results indicate that initially, while a short still remains as a high-resistance ISC, the ISC joule heats are similar among all the tested cases. This is because, for large-resistance shorts, the amount of short current that flows through an ISC is mainly determined by the short itself. However, once an ISC evolves into a low-resistance short, the short current starts to be limited by kinetics and transport in the battery. Therefore, joule heats for a short show significant departures among the cases when the ISC gets into a range of low resistances. For a low-resistance short, a larger capacity battery can provide higher current for an ISC, generating much higher joule heat around the short. On the other hand, the joule heat for a similar short in a small-capacity battery is much less. However, it should be noted that large overpotentials for kinetic and concentration limitations contribute significant amounts of heat during the low-resistance short discharge process in small-capacity batteries. The differences between the dotted lines and the solid lines of each color in Fig. 11 indicate the amount of reduction in the ISC joule heat for corresponding module capacities. This implies that introducing a resistive balance path among parallel cell units significantly slows down the electrical energy feed into a faulty cell from the other healthy cells in a module.

4. Fault isolation

Even though electrical isolation of a fault is a common practice in a general electrical system to prevent the system from feeding electrical energy into a fault, both an active circuit-breaker such as a switch and a passive circuit-breaker such as a fuse do not easily work in typical large-capacity LIB systems. However, as suggested in the previous section, the concept proposed here facilitates a methodology for detection of a fault even in large LIBs, opening an opportunity to introduce active circuit-breakers.
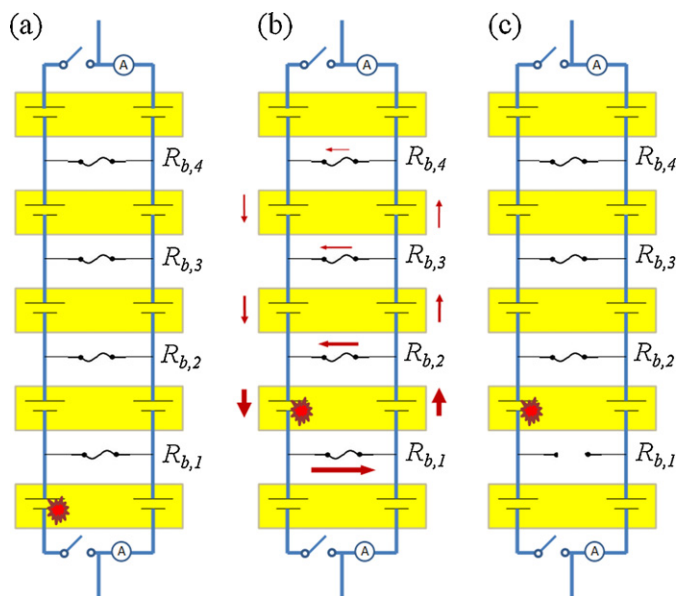
Fig. 12 illustrates isolation of faulted cells using a combination of active and passive circuit-breakers. In Fig. 12a, the ISC occurs at cell (1,1), which is directly connected to a module terminal. Once this fault is detected using the signal suggested in Eq. (1), the faulted series branch can be disconnected from the module terminals by opening the switches at the terminals as illustrated in the diagram. If the fault occurs at the cell connected to one of the terminals, the faulted cell is immediately electrically isolated as soon as the switches are open. If a fault occurs in a cell that is not directly connected to a terminal (Fig. 12b), the fault is not immediately isolated when the faulted branch is disconnected from the terminals. When the switches are still closed, the fault-feeding system current is mostly carried by conductive power lines along the series branches. Once the switches are open, the system fault current is carried through the balance line resistors as seen in Fig. 12b. Because the system fault current flowing through the balance line resistors is now much larger than the normal balance current, a passive circuit-breaker such as a fuse can be applied to open the balance lines. Once the balance lines on either side of the faulted cell open, the cell becomes electrically isolated, as illustrated in Fig. 12c.

Fig. 13 shows simulations of the system response when the faulted branch in Fig. 12b becomes disconnected. In the simulated case, an ISC occurs at 5 s in cell (1,2) of a 40-Ah (20 Ah + 20 Ah) module. Balancing lines use 0.1-Ω resistors. The number of cells in a series branch is five. The signals at the positive and negative terminals of the module are plotted in Fig. 13a for a 0.1-Ω ISC. The faulted branch is disconnected from the module terminals by opening the switches on the branch at 10 s. The balance line currents during the short event simulated are shown in Fig. 13b. The balance resistor currents are an order of magnitude smaller than the fault signal current. This implies that current induced by a fault is mostly carried by conductive series branches through the module terminals as intended. Because the module is well balanced initially, the balance lines do not carry current until an ISC occurs at 5 s. When the terminal switches are open at 10 s, the resistor $R_{b,1}$ starts to carry the largest current so the sum of the resistor currents is zero. If electric fuses are applied in the balance resistors, $R_{b,1}$ would open first, isolating the faulted cell (1,2). Once the faulted cell is successfully electrically isolated, the subsequent behavior of the faulted cell depends on the characteristics of the individual unit cell and
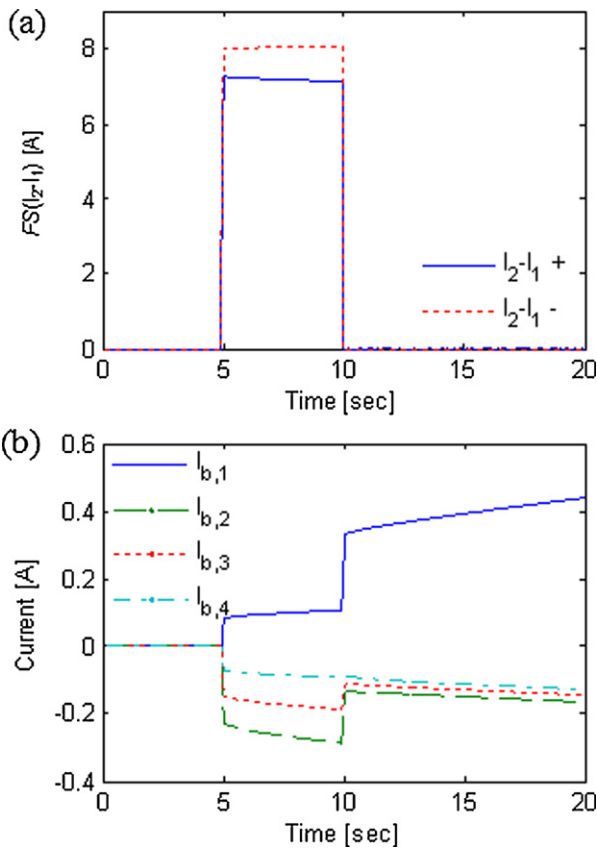
Fig. 13. Pack ISC simulation results of (a) fault signals (*FS*) at positive and negative module terminals, and (b) balance resistor currents for a 0.1 Ω ISC. ISC occurs at 5 s in cell (1,2) of the module with conditions $C_{mdl} = 40$ Ah (20 Ah + 20 Ah), $I_{mdl} = 0$ A, $N_s = 5$, $R_b = 0.1$ Ω. The faulted series branch is disconnected by opening switches at module terminals at 10 s.
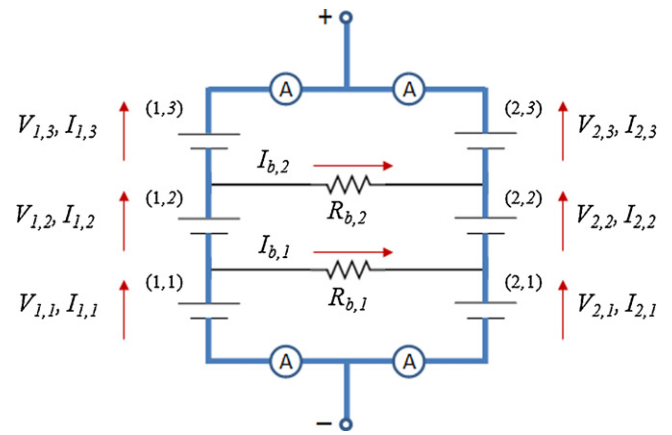

Fig. 14. Circuit diagram of experimental setup.

not on the pack or module assembly characteristics. Therefore, pack safety issues can possibly be reduced by designing a safe unit cell. As inferred from the diagrams in Fig. 12, the multiple series-branch configuration of the proposed design allows partial power delivery from the pack even after the local shutdown of fault isolation is executed.

5. Experimental demonstration

An experimental setup is used to demonstrate the proposed concept. The demonstration module consists of two parallel sets of three Dow Kokam 8-Ah SLPB75106100 lithium polymer cells in series, as shown in Fig. 14. Balance resistors with appropriate power ratings for short circuit balancing are used for different test cases. To simulate short conditions, power resistors with various ohmic ratings are connected across the terminals of the shorted cell via a relay. All test cases are conducted with the cells fully
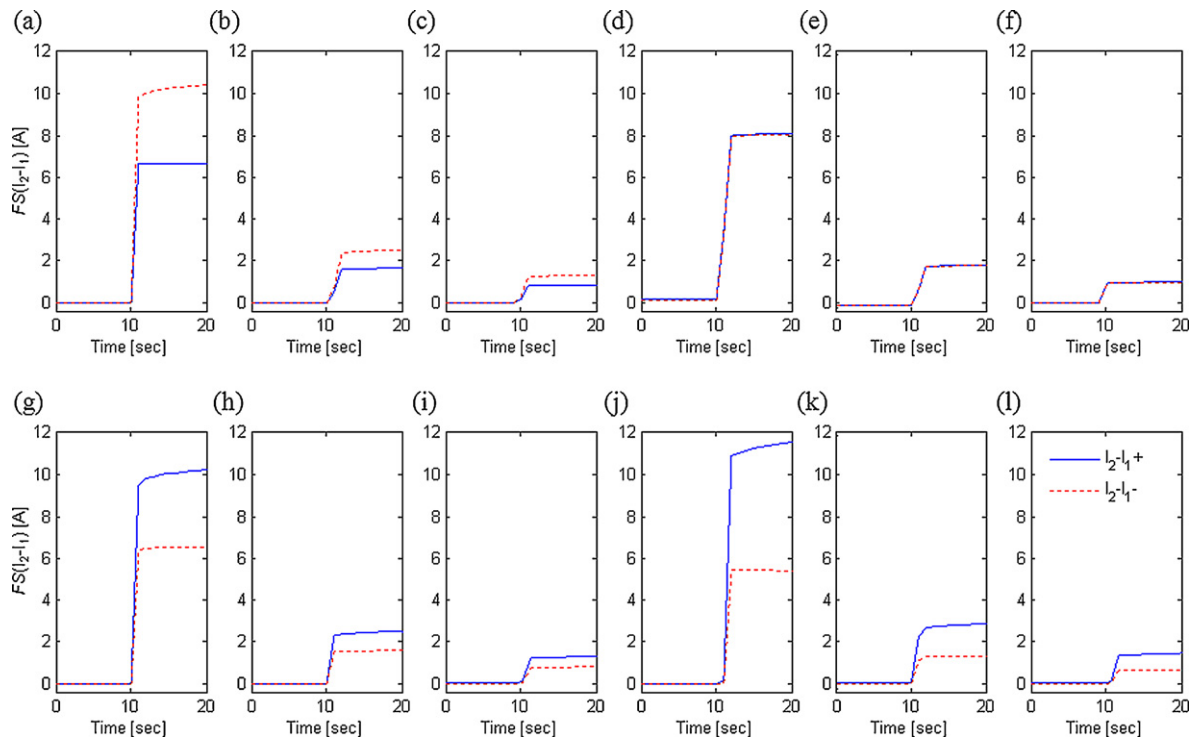

Fig. 15. Experimental results of fault signals (*FS*) at positive and negative module terminals (a) for a 0.1-Ω ISC, (b) for a 0.5-Ω ISC, and (c) for a 1-Ω ISC induced in cell (1,1) in a module with conditions, $C_{mdl} = 16$ Ah (8 Ah + 8 Ah), $I_{mdl} = 0$ A, $N_s = 3$, $R_b = 0.2$ Ω; same with (d), (e), (f) for ISCs induced in cell (1,2); same with (g), (h), (i) for ISCs induced in cell (1,3); same with (j), (k), (l) ISCs induced in cell (1,3) and $R_b = 0.1$ Ω.

Table 3
Summary of control parameters for the module short tests with the proposed design.

	a	b	c	d	e	f	g	h	i	j	k	l
Faulted cell	(1,1)	(1,1)	(1,1)	(1,2)	(1,2)	(1,2)	(1,3)	(1,3)	(1,3)	(1,3)	(1,3)	(1,3)
R_s [Ω]	0.1	0.5	1.0	0.1	0.5	1.0	0.1	0.5	1.0	0.1	0.5	1.0
R_b [Ω]	0.2	0.2	0.2	0.2	0.2	0.2	0.2	0.2	0.2	0.1	0.1	0.1

charged and with an initial voltage variation of no more than 10 mV. For this series of tests, all measurements are taken during a rest with no charge or discharge current applied to a module. Data are acquired with a National Instruments CompactDAQ using Lab-view software. Measurements are taken at 1-second intervals for all points. Measurements include cell voltages, shunt voltages, and balance resistor voltages. Four 10-A current shunts are installed at the four corners of the module terminals, as shown in Fig. 14. Both the balance and short resistors are within 1% tolerance to ensure the accuracy of the test results. Tests are composed of 10 s of static data followed by a short event.

Fig. 15 presents measured fault signals (Eq. (1)) from twelve separate experiments for which faulted-cell location in the module, ISC resistance, and balance resistance are individually varied. Table 3 summarizes the values of the parameters for the 12 cases presented. Fig. 15a, 15b, and 15c compare the signals from different resistance shorts, 0.1-Ω, 0.5-Ω, and 1-Ω ISCs, when a short occurs in cell (1,1) with 0.2-Ω balance resistors between the series branches. As expected from model predictions, the magnitude of the fault signal is a strong function of the ISC resistance, and the magnitude is larger at the negative terminal, as it is closer to the faulty cell than the positive terminal is. The signals are clear for detection even for a 1-Ω ISC, which represents a short in its early stage of evolution. Fig. 15d–f present the same cases for a short occurring in cell (1,2). Because the faulty cell is located at the exact middle of the module, the fault signals measured at the positive and negative terminals are shown to be identical. Fig. 15g–i present the same cases for a short occurring in cell (1,3). In these cases, the faulty cell is closer to the positive terminal of the module, producing a larger signal at the positive side than at the negative side. Compared with the cases shown in Fig. 15a–c, the signals from positive and negative sides of the module are interchanged due to the symmetry of the locations of the faults in the module. Fig. 15j–l present the same cases shown in Fig. 15g–i except that the resistance of balance resistors is reduced to 0.1 Ω. Because the balance resistors carry increased current in the positive direction for the sign denoted in Fig. 14, the fault signal from the positive side of the module increases in magnitude, while it decreases at the negative side of the module.
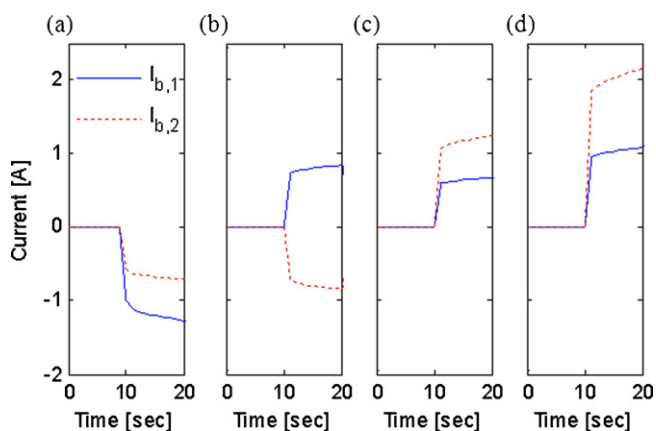
The balance resistor currents are plotted in Fig. 16. The magnitudes and signs of the balance currents are functions of the faulted-cell location, the resistance of the balance resistors, and the ISC resistance. The currents of the balance resistors are an order of magnitude smaller than the fault signals measured at the module terminals. Overall, the observations from the experimental demonstration of the concept confirm the model analysis for the functionality and viability of the proposed fail-safe design and method for large-capacity LIB systems.

6. Conclusion

A fail-safe design for large-capacity LIB systems is presented. The proposed design separates the distinctive functions of electric pathways in LIBs by carrying a large electric current along conductive series branches and by carrying moderate parallel balance current across resistive balance lines. This facilitates a robust methodology for early stage detection and isolation of a fault in a large-capacity LIB, enhancing its safety. The increased fault signal can be easily detected using measurements at the module terminals when a fault occurs in one of the unit cells. A pack ISC response model analysis reveals that the magnitude of the signal is a strong function of the resistance of an induced ISC; the module output current does not greatly affect the signal proposed; the magnitude of the signal decreases slowly as the number of cells in series in a module increases; the ratio of the signals at the positive terminal and the negative terminal varies with the location of a faulted cell in a module; the signal proposed is easier to sense in a larger capacity and a higher power module. Therefore, using the signal from the fail-safe design proposed, the status of ISC evolution in a large LIB system can be determined by the on-board battery management system, and the defective cell in a module can be located so that the fault can be addressed locally. A detected faulty cell can be electrically isolated using active and passive circuit breakers with the design suggested to prevent the system from feeding further electrical energy into the fault. Once the faulty cell is successfully electrically isolated, the subsequent behavior of the faulted cell depends on the characteristics of that individual unit and not on the pack assembly characteristics. Experimental demonstration confirms the findings from the pack ISC model analysis and demonstrates viability of the proposed fail-safe design.

Fig. 16. Experimental results of balance resistor currents for an ISC induced (a) in cell (1,1), (b) in cell (1,2), (c) in cell (1,3) in a module with $R_b = 0.2$ Ω; same with (d) for 0.1-Ω ISC induced in cell (1,3) in a module with $R_b = 0.1$ Ω.

References

[1] http://www.ntsb.gov/doclib/reports/2005/HZB0501.pdf.
[2] E.P. Roth, D.H. Doughty, J. Power Sources 128 (2004) 308–318.
[3] T.D. Hatchard, D.D. MacNeil, A. Basu, J.R. Dahn, J. Electrochem. Soc. 148 (2001) A755–A761.
[4] R. Spotnitz, J. Franklin, J. Power Sources 113 (2003) 81–100.
[5] G.-H. Kim, A. Pesaran, R. Spotnitz, J. Power Sources 170 (2007) 476–489.
[6] G.-H. Kim, K. Smith, A. Pesaran, 5th Int. Sym. Large Li-ion Battery Tech. and Appl., June 9–10, 2009, Long Beach, CA.

[7] S. Santhanagopalan, P. Ramadass, J. Zhang, J. Power Sources 194 (2009) 550–557.
[8] K. Smith, G.-H. Kim, E. Darcy, A. Pesaran, Int. J. Energy Res. 34 (2010) 204–215.
[9] R. Srinivasan, J. Power Sources 198 (2012) 351–358.
[10] R. Srinivasan, B.G. Carkhuff, M.E. Butler, A.C. Baisden, Electrochim. Acta 56 (2011) 6198–6204.
[11] C. Mikolajczak, J. Harmon, K. White, Q. Horn, M. Wu, Power Electronics Technology, March 2010.
[12] R. Yazami, 6th Lithium Mobile Power, Boston, MA, November 4–5, 2010.
[13] T. Fuller, M. Doyle, J. Newman, J. Electrochem. Soc. 141 (1994) 1–10.
[14] K.A. Smith, C.D. Rahn, C.-Y. Wang, Energy Convers. Manage. 48 (2007) 2565–2578.